Structural Engineering and Mechanics, *Vol. 51, No. 4 (2014) 581-599*
DOI: http://dx.doi.org/10.12989/sem.2014.51.4.581

Dynamic effect of high-speed trains on simple bridge structures

Christoph Adam* and Patrick Salcher[a]

Department of Civil Engineering Science, Unit of Applied Mechanics, University of Innsbruck, 6020 Innsbruck, Technikerstraße 13, Austria

(Received March 24, 2011, Revised April 16, 2014, Accepted May 3, 2014)

Abstract. In this paper the overall dynamic response of simple railway bridges subjected to high-speed trains is investigated numerically based on the mechanical models of simply supported single-span and continuous two-span Bernoulli-Euler beams. Each axle of the train, which is composed of rail cars and passenger cars, is considered as moving concentrated load. Distance, magnitude, and maximum speed of the moving loads are adjusted to real high-speed trains and to load models according to Eurocode 1. Non-dimensional characteristic parameters of the train-bridge interaction system are identified. These parameters permit a spectral representation of the dynamic peak response. Response spectra assist the practicing engineers in evaluating the expected dynamic peak response in the design process of railway bridges without performing time-consuming time history analyses.

Keywords: dynamic peak response; high-speed train; response spectra; train-bridge interaction

1. Introduction

If a train passes a railway bridge with high constant speed, the bridge may be driven into a condition of resonance. Since many decades this effect is well known, and thus, numerous analytical and numerical models of different degree of sophistication have been developed aiming at predicting the dynamic bridge response, see e.g., (Fryba 1996, 2001, Yang *et al*. 1997, Museros and Alarcon 2005, Xia *et al*. 2006, Liu *et al*. 2009). Some of these studies have been supported by experimental investigations, see e.g., (Zambrano 2011). More recently, the construction of railways for high-speed trains has led to intensified research efforts, because the travel speed up to 320 km/h combined with increasing bridge spans induces increased demands on bridge structures (Museros and Alarcon 2005). The textbook of Yang *et al*. (2004) provides a comprehensive state-of-the-art report of methods for the analysis of vehicle-bridge interaction dynamics with emphasis on applications to high-speed railways.

Simultaneously, Hauser and Adam (2007), Fink and Mähr (2007) have introduced a methodology, which permits a quick and yet accurate assessment of the maximum dynamic railway bridge response subjected to high-speed trains without performing expensive time history analyses.

*Corresponding author, Professor, E-mail: christoph.adam@uibk.ac.at
[a]Ph.D. Student, E-mail: Patrick.salcher@uibk.ac.at

http://www.techno-press.org/?journal=sem&subpage=8 ISSN: 1225-4568 (Print), 1598-6217 (Online)

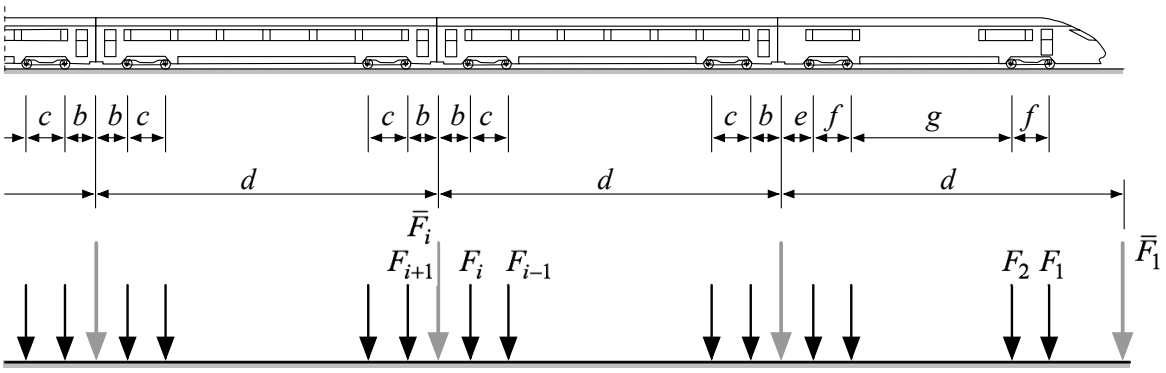

Fig. 1 Idealization of the train loads. Black: Consideration of each axle as moving load. Grey: Simplified consideration – merging the individual axle loads close to both ends of the carriages into a single moving concentrated load

In this study spectral representations of the high-speed train induced dynamic peak response, in the following referred to as response spectra, are derived for simply supported single-span and continuous two-span *Bernoulli-Euler* beam models subjected to a series of moving loads with constant speed. Distance, magnitude and maximum speed of the moving loads is adjusted to real high-speed trains according to Eurocode 1 (Eurocode 1 2003). Subsequently, response spectra are presented for the peak deflection, the peak acceleration response, and peak bending moment. Other example problems may be found in (Salcher 2010).

2. Modeling of train-bridge interaction

2.1 Idealization of the train loads

In the most general approach the train vehicle may be modeled with different degree of sophistication as a spring-mass system consisting of the car body, bogies, and visco-elastic connection elements, as outlined e.g., in (Liu *et al*. 2009). However, it has already been mentioned by Museros and Alarcón (2005) that sophisticated train models have beneficial effects on the bridge response, because they operate like a Tuned Mass Damper, which reduce the vibration amplitudes of the bridge. Since in the design process of a bridge the properties of all passing trains to be developed during the bridge life cycle are not known, analysis should not be performed considering particular characteristics of the vehicle (Museros and Alarcón 2005).
Thus, for the present study each axle of the train, which is composed of rail cars and passenger cars, is considered as a moving concentrated load with constant speed v. Thereby, each concentrated load corresponds to the static reaction force of an axle. In Fig. 1 the axle loads are displayed in black and denoted by F_i, F_{i+1}, etc. In such a model the inertia effect of the train in the interaction system of moving train and bridge is neglected.

Depending on the type of high-speed train each passenger car can be supported by a bogie at the front and at the rear with two axles. Alternatively, the rear bogie and the front bogy of two adjacent cars can be merged into a single bogie with two axles or one axle (Museros and Alarcón 2005). Consequently, the mechanical train model consists of a sequence of lateral group loads or of

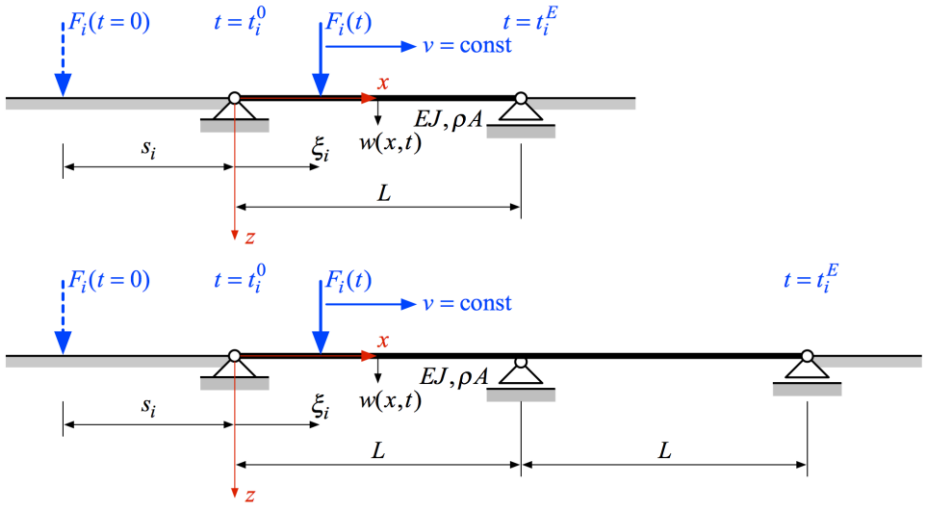

Fig. 2 Moving lateral load with constant speed passing a simply supported single-span and a two-span continuous beam, respectively

single lateral loads (for the latter trains), which pass the bridge with constant speed. In several studies lateral group loads are merged to a single load (e.g., $\bar{F}_i$), as shown in Fig. 1 in grey. This simplification is also evaluated in the present study.

2.2 Considered trains

2.2.1 Input parameters

Besides the train speed and the load magnitude, distance *d* of the concentrated loads and/or load groups (see Fig. 1) is a further critical parameter for dynamic bridge excitation. Load magnitude and distance depend on the type of train. The considered train types are subsequently discussed.

2.2.2 Load model for the ICE ET 410 train

Here, several studies are performed utilizing a simplified model of the high-speed train ICE ET 410. The example train, which is subsequently referred to as long train, is composed as follows: 1 rail car - 7 passenger cars - 1 rail car - 6 passenger cars. The second considered example train, which is referred to as short train, has one rail car followed by seven passenger cars. Each car has at both ends a bogie with two axles each. The distances of the axles according to Fig. 1 are: b=2.27 m, c=2.80 m, d=24.34 m. It is assumed that the length of the rail cars correspond to the distance d of the passenger cars, compare with Fig. 1. The axle loads of the rail cars are 200 kN, the axle loads of the passenger cars are 116.5 kN. As already mentioned, for comparative studies the axle loads at the front end and the rear end of the adjacent vehicle are merged into a single concentrated load, compare also with Fig. 1.

2.2.3 Set of European high-speed trains

High-speed trains, which are authorized in Europe for operating bridges, are considered in this study as a train set. This train set contains conventional trains (e.g., ICE, Railjet), articulated trains

(e.g., TGV, Thalys, Eurostar), and regular trains (Talgo) (Eurocode 1 2003). The corresponding load models comprising the combination of rail and passenger cars, number of cars, axles loads, car length, and axles distances are outlined in (Salcher 2010).

2.2.4 HSLM-A train set according to Eurocode 1

According to Eurocode 1 (2003) the high-speed load models (HSLM) A1 to A10 must be utilized for the dynamic analysis of railway bridges, besides the European train set. This set of load models is valid for bridges with a span larger than 7 m. The individual models A1 to A10 consider different magnitudes of axle loads, car length, bogie distances, and number of cars. For details see (Eurocode 1 2003, Salcher 2010).

2.3 Bridge model

In the present study the considered simply supported single-span and continuous two-span bridges are modeled as linear elastic *Bernoulli-Euler* beam of constant mass per unit length ρA and constant bending stiffness EJ, see Fig. 2. The ith axle load F_i, which passes the bridge with constant speed v, induces lateral vibrations $w(x,t)$. $w(x,t)$ is governed by the following equation of motion (Museros and Alarcon 2005, Hauser and Adam 2007)

$$\rho A\,\ddot{w} + EJ\,w_{,xxxx} = F_i\,\delta(x-\xi_i)\left[H(t-t_i^0) - H(t-t_i^E)\right] \tag{1}$$

t denotes the time variable. In Eq. (1) *Dirac* delta function δ determines the location x_i of the lateral force at time t on the bridge. Unit step function H indicates, when F_i arrives and departs the beam at time instants t_i^0 and t_i^E, respectively. The actual location x_i of F_i and time instants t_i^0 and t_i^E depend on the speed v and the initial location s_i according to

$$\xi_i = v\,t - s_i \quad , \quad t_i^0 = \frac{s_i}{v} \quad , \quad t_i^E = \frac{s_i + l}{v} \tag{2}$$

compare also with Fig. 2. For a single-span beam $l=L$, for the two-span beam $l=2L$.

For the solution of Eq. (1) the lateral displacement w is split into its quasistatic part w_S and its complementary dynamic counterpart w_D (Adam 1999)

$$w = w_S + w_D \tag{3}$$

Since the quasistatic response w_S can be expressed in closed form, only the complementary dynamic response is found by modal analysis (Adam 1999). Modal decomposition of $w_D(x,t)$ into the mode shapes $\phi_n(x)$ of the actual beam problem (Clough and Penzien 1993, Ziegler 1998)

$$w_D(x,t) = \sum_{n=1}^{\infty} Y_n(t)\,\phi_n(x) \tag{4}$$

leads to an infinite set of ordinary oscillator equations of motions for the complementary modal coordinates $Y_n(t)$, see e.g., (Adam *et al*. 2000)

$$\ddot{Y}_n + 2\zeta_n\omega_n\dot{Y}_n + \omega_n^2 Y_n = -\frac{1}{m_n\omega_n^2}\left(\ddot{P}_n^i + 2\zeta_n\omega_n\dot{P}_n^i\right) \quad , \qquad n = 1,\ldots,\infty \quad , \tag{5}$$

$$P_n^i(t) = F_i\,\phi_n(x = v\,t - s_i)\left[H(t - \frac{s_i}{v}) - H(t - \frac{s_i + l}{v})\right]$$

m_n is the nth modal mass

$$m_n = \rho A \int_l \phi_n{}^2(x)\mathrm{d}x \tag{6}$$

and ω_n denotes the nth natural circular frequency of the beam.

For a simply supported single-span beam the modal properties are derived as (Clough and Penzien 1993)

$$\omega_n = \frac{n^2\pi^2}{L^2}\sqrt{\frac{EJ}{\rho A}},\ \phi_n(x) = \sin\frac{n\pi x}{L},\ m_n = \frac{\rho A L}{2} \tag{7}$$

The natural frequencies and the mode shapes of the two-span continuous beam can be separated into two groups (Blevins 2001, Wang *et al*. 2010),

$$\omega_n = \beta_n^2\sqrt{\frac{EJ}{\rho A}},\ \beta_n = \begin{cases}(n+1)\pi/(2L), & n = 1,3,5,7,..\\ (1/2+n)\pi/(2L), & n = 2,4,6,8,..\end{cases} \tag{8}$$

$$n = 1,3,5,7,\ldots:\ \phi_n(x) = \sin(\beta_n x)\sqrt{\frac{EJ}{\rho A}}$$

$$n = 2,\ 4,\ 6,8,\ldots:$$

$$\phi_n(0 \le x \le L) = \sin(\beta_n x) - \frac{\sin(\beta_n L)}{\sinh(\beta_n L)}\sinh(\beta_n x) \tag{9}$$

$$\phi_n(L \le x \le 2L) = \frac{\sin(\beta_n L) + \sinh(\beta_n L)}{\cos(\beta_n L) + \cosh(\beta_n L)}\left[\cosh(\beta_n x) - \cos(\beta_n x)\right] + \sin(\beta_n x) - \sinh(\beta_n x)$$

For odd numbers of n the modal properties correspond to those of a simply supported beam. The additional natural frequencies at even numbers of n consider the continuity of the beam at the intermediate support.

In Eq. (5) the effect of structural damping has been considered by modal adding of viscous damping ζ_n (Adam *et al*. 2000, Ziegler 1998). Structural bridge damping is a fundamental bridge parameter, in particular for excitation at resonance. In (Eurocode 1 2003) lower limit values for viscous damping are defined. They depend on the type of bridge and span L, compare with Table 1.

The solution of the quasistatic part w_S can be expressed in closed form, and only the infinite modal series of the complementary dynamic part, Eq. (4), needs to be approximated by a finite number of N modes. It has been shown (Adam 1999) that such a procedure accelerates the rate of convergence of the modal series, or even ensures convergence, if response quantities contain derivatives of the displacement w of higher order. In this study, the N modal coordinates, Eq. (5), have been derived in the time domain by application of *Duhamel* integral (Clough and Penzien 1993). For details see Salcher (2010). The response of the beam loaded by a train of N axles is found by superposition of the individual responses for each load F_i.

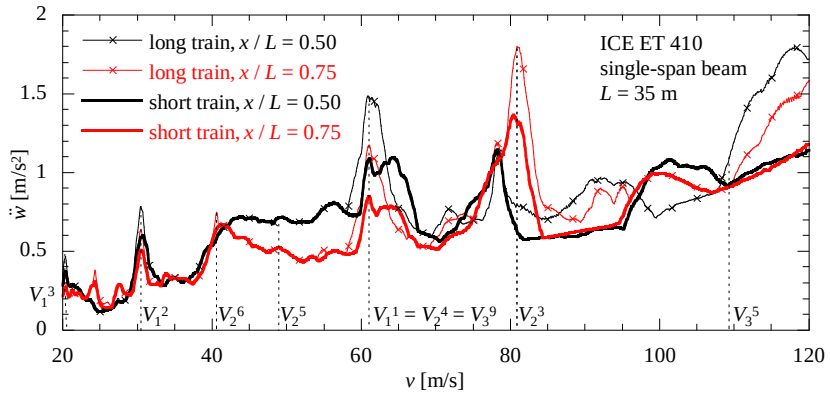

Fig. 3 Peak acceleration at mid-span and at 0.75L plotted against the train speed. Single-span bridge, fundamental frequency f_1=2.50 Hz. Two different configurations of the high-speed train ICE ET 410

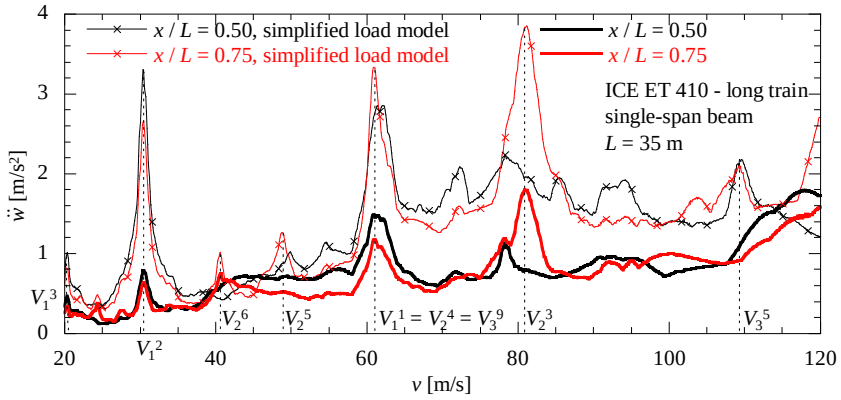

Fig. 4 Peak acceleration at mid-span and at 0.75L plotted against the train speed. Single-span bridge, fundamental frequency f_1=2.50 Hz. High-speed train ICE ET 410: Load model containing each axle load, and simplified load model with merged axle loads at the car ends

3. Critical train speeds

At critical train speeds v the dynamic response of the bridge is severely amplified, and the bridge is driven into resonance. The main source of bridge resonance is the rhythmic repetition of moving forces with constant speed. The corresponding critical speeds of concentrated forces with the same magnitude and with distance d are determined according to the relation (Yang *et al*. 2004, Museros and Alarcon 2005)

$$V_n^i = \frac{d\,\omega_n}{2\pi i} \equiv \frac{d\,f_n}{i} \quad , \quad n = 1,2,3,... \quad , \quad i = 1,2,3,... \tag{10}$$

They depend on the linear natural beam frequencies $f_n=\omega_n/(2\pi)$, and on the length d of the rail cars.

Resonance may be also induced by the constant speed of the moving forces itself. For a simply supported beam the following relation for the critical speeds (of second order) $\bar{V}_n$ is derived (Ziegler 1998, Fryba 2001)

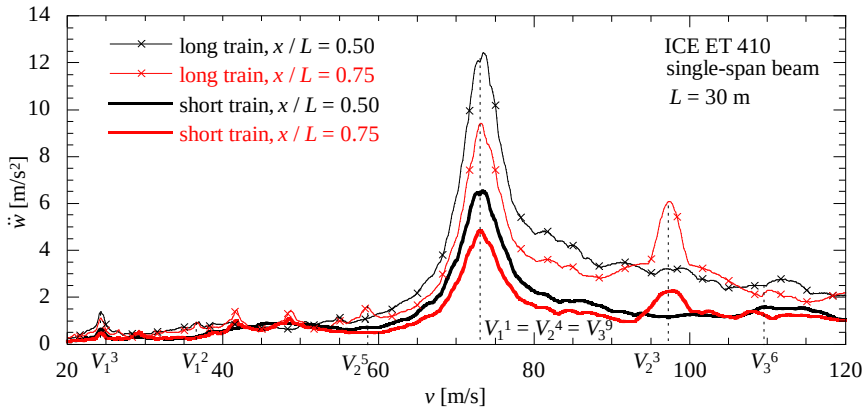

Fig. 5 Peak acceleration at mid-span and at 0.75L plotted against the train speed. Single-span bridge, fundamental frequency f_1=3.00 Hz. Two different configurations of the high-speed train ICE ET 410

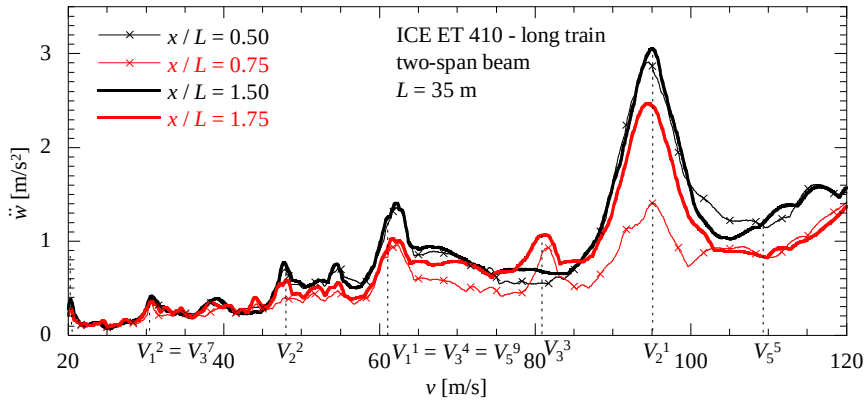

Fig. 6 Peak acceleration at 0.50L, at 0.75L, at 1.50L and 1.75L plotted against the train speed. Two-span bridge, fundamental frequency f_1=2.50 Hz. High-speed train ICE ET 410

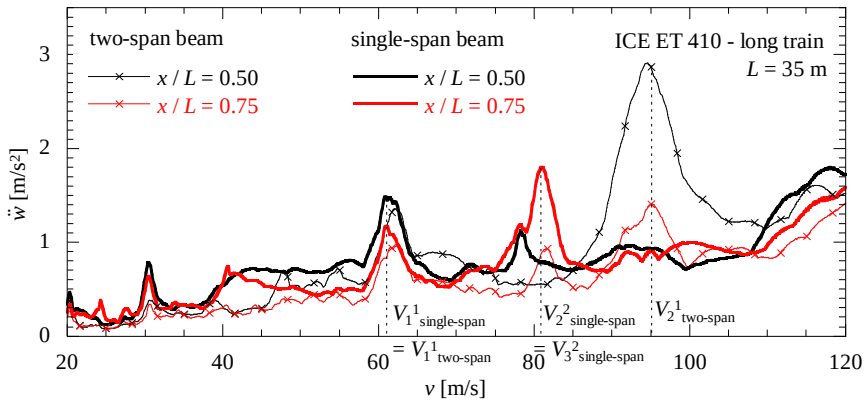

Fig. 7 Peak acceleration at 0.50 L, and at 0.75 plotted against the train speed. Single span bridge versus two-span bridge, fundamental frequency f_1=2.50 Hz. High-speed train ICE ET 410

$$\bar{V}_n = \frac{2L\omega_n}{2\pi n} \equiv \frac{2Lf_n}{n} \quad , \quad n = 1,2,3,... \tag{11}$$

In general critical speeds $\bar{V}_n$ are not hit by high-speed trains, and are thus not of significance in the present study.

Furthermore, sway forces of the train vehicles induced by track irregularities and wheel hunting movements may lead to periodical actions on the bridge, and subsequently to bridge resonance (Xia *et al*. 2006). However, this type of resonance is out of scope of the present investigation.

4. Example problems

In the first example problem a simply supported bridge with the following parameters is utilized: span L=35.0 m, mass per unit length ρA=20,000 kg, bending stiffness EJ=7.603E+10 Nm^2, damping coefficients ζ_n=0.01 (n =1,2,…). The corresponding fundamental bridge frequency is f_1=2.5 Hz. According to Eq. (10) critical speeds (of first order) in the speed range between 0 and 120 m/s can be derived as: V_1^1=60.9 m/s, V_1^2=30.4 m/s, V_1^2=20.3 m/s, V_2^3=81.1 m/s, V_2^4=60.9 m/s, V_2^5=48.7 m/s. The critical speed (of second order) $\bar{V}_1$=175 m/s is larger than the maximum speed of the considered train. In the time-history response analysis the first three modes (i.e., n=1,2,3) are considered.

Fig. 3 shows the maximum bridge acceleration at mid-span and at three-quarters of the span as function of the train speed v. Bridge vibrations are induced by the load models of the ICE ET 410 train, as described in section 2.2.2. The short train consists of 1 rail car and 7 passenger cars, while the long train includes 1 more rail car and 6 more passenger cars. It can be seen that the peaks of the maximum response occur principally at critical speeds although repetitive groups of four axle forces pass the bridge. Since the long train excites the bridge periodically for a longer time period, at certain speed ranges the maximum acceleration response is larger than for the short train, in particular at critical speeds. It is interesting to observe that for a critical speed of V_2^3 the peak response at three-quarters of the span is a maximum in the considered speed range, i.e., larger than at mid-span. This response behavior can be led back to higher mode effects, i.e., at certain speeds and at certain bridge locations the second mode contributes significantly to the acceleration response. Thus, the second mode must be considered in the analysis of the acceleration.

In Fig. 4 the peak bridge accelerations induced by the long train are set in contrast to the outcomes of an analysis, where the axle loads of the adjacent car ends are merged to a single load. It can be observed that this simplification leads to over-conservative response predictions at critical speeds. E.g., at V_1^2 the simplified derived maximum acceleration is more than four times larger than the one based on load model considering each axle load separately.

In the next study the bridge length L is reduced to 30 m. The fundamental frequency increases to f_1=3.0 Hz. All other bridge and excitation parameters remain unchanged. From Fig. 5 it can be seen that the maximum peak response is associated to the fundamental critical speed V_1^1. It is interesting to observe that the maximum response of 12.5 m/s^2 is much larger than for the previously considered bridge with 3.8 m/s^2.

The peak accelerations at four locations of a continuous two-span bridge with spans of L=35.0 m are shown in Fig. 6. All other parameters are identical to single-span bridges. The considered locations are both mid-spans and three-quarters of the spans. In order to cover the same

frequency range as in the corresponding single-span bridge the first five modes are included in the time-history analyses. At both mid-spans the response is larger compared to the peak acceleration at the three-quarter points except for the critical speed V_3^3.

Comparison of the outcomes of this bridge with the results of the corresponding single-span bridge reveals that in the lower speed range the response of the single-span bridge is larger. However, at the critical speed V_2^1 of the two-span bridge, which is associated to the second mode, the peak acceleration at mid-span of the first field exceeds the corresponding response of the single-span bridge dramatically, see Fig. 7. The reason is that this mode does not existent for the single-span bridge.

5. Response spectra

5.1 Characteristic parameters

The excitation frequency of the moving train can be expressed in terms of the constant speed as $\pi v/L$ (Yang *et al*. 1997, Yang *et al*. 2004). Relating this excitation frequency to the fundamental natural beam frequency ω_1 leads to the definition of the non-dimensional speed parameter S (Yang *et al*. 1997, Yang *et al*. 2004)

$$S = \frac{\pi v}{\omega_1 L} \equiv \frac{v}{2 f_1 L} \tag{12}$$

In several studies, e.g., (Yang *et al*. 1997, Yang *et al*. 2004), the dynamic response due to the effect of inertia has been presented by an impact factor, which expresses the magnification of the dynamic response compared to the corresponding static one. This factor is only useful when response quantities (such as the deflection w and the bending moment M_y) are considered, which also arise in statically loaded structures. However, the bridge acceleration $\ddot{w}$ is an essential response parameter, which also needs to be assessed by the practicing engineer (Museros and Alarcon 2005). Hence, for the present study the following non-dimensional response quantities are utilized (Hauser and Adam 2007, Salcher 2010)

$$\bar{\ddot{w}} = \ddot{w}\frac{\rho A L}{F_{\max}} \quad , \quad \bar{w} = w\frac{EJ}{F_{\max} L^3} \quad , \quad \bar{M}_y = \frac{M_y}{F_{\max} L} \tag{13}$$

Here, $F_{\max}$ is the maximum axle load of the considered load model. A non-dimensional characteristic length of this dynamic problem is the ratio L/d composed of bridge-span L and car length d.

As previously discussed, the peak response depends strongly on the critical speed. Since a train may pass a bridge with a speed starting from (almost) zero to a maximum admissible (non-dimensional) speed S_0=max$S$, the maximum response in the speed range $0 \le S \le S_0$ is of particular interest

$$\bar{\ddot{w}}_0(S_0) = \max|\bar{\ddot{w}}|(S \le S_0) \quad , \quad \bar{w}_0(S_0) = \max|\bar{w}|(S \le S_0) \, , \quad \bar{M}_{y,0}(S_0) = \max\left|\bar{M}_y\right|(S \le S_0) \tag{14}$$

In the following the peak response is specified as a function of the maximum admissible speed parameter S_0 according to the definitions of Eq. (12).

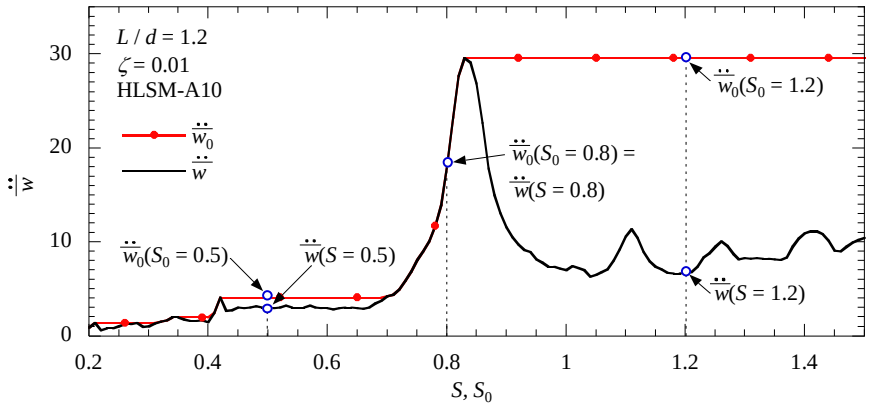

Fig. 8 Definition of the peak acceleration response. $\ddot{\bar{w}}$ is the peak response at a certain speed parameter S. $\ddot{\bar{w}}_0$ denotes the peak response in range of speed parameters $0 \le S \le S_0$

Note that the response at the speed parameter S (except $\ddot{\bar{w}}(S) = \ddot{\bar{w}}(S_0)$) is of no significance for estimating the peak bridge response. Fig. 8 illustrates for an example problem the difference between $\ddot{\bar{w}}_0(S_0)$ and $\ddot{\bar{w}}(S)$.

5.2 Definition of response spectra

These parameters permit the three-dimensional representation of the dynamic peak response as function of the maximum admissible speed parameter S_0 and the normalized length L/d. Since S_0 contains the fundamental bridge frequency, the results are referred to as response spectra (in analogy to earthquake engineering). Here, response spectra are presented for peak displacement, peak acceleration, and peak bending moment. The concept of response spectra for railway bridges has been introduced simultaneously by Hauser and Adam (2007), Fink and Mähr (2007). Note that already Yang *et al*. (1997) have presented the actual dynamic impact factor as function of the speed parameter S and the normalized length L/d for the mid-span deflection. The advancement of the response spectrum methodology compared to the presentation of (Yang *et al*. 1997) is that the maximum peak response, which occurs in the complete range of admissible speeds at any point, is specified. Response spectra based on a set of European high-speed trains and on the HSLM-A trains are derived separately for single-span and continuous two-span bridges.

In the compilation process of response spectra various time history analyses for various bridge-train combinations are performed. In each analysis the response at closely spaced discrete points of the span is determined, and the peak response is recorded (which may occur at other locations than at mid-span). From this it follows that the spectral response quantities of the spectra cannot be related to a certain beam location. The peak response is plotted against the corresponding maximum admissible speed parameter S_0 and the normalized length L/d. Response spectra are determined for each train model. Subsequently, envelope spectra are determined for two groups of trains: Envelope response spectra based on a set of European high-speed trains and on the HSLM-A trains are derived separately for single-span and two-span bridges. If envelope response spectra are readily available, the practicing engineer can assess quick and yet accurate the peak bridge

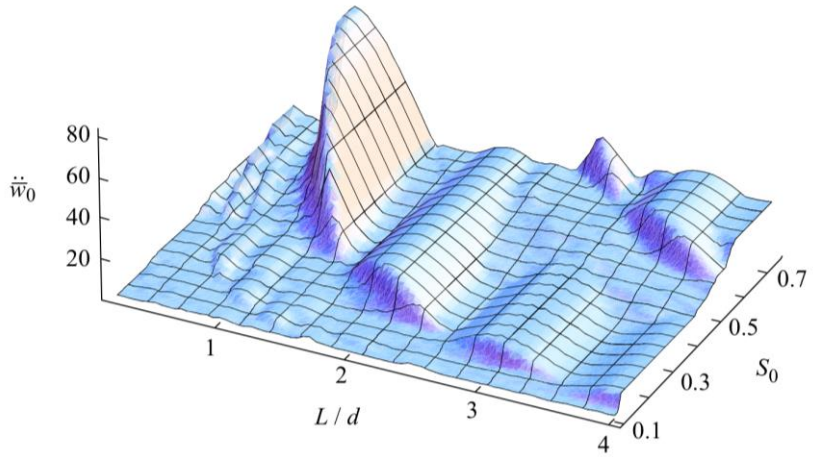

(a) Acceleration response spectrum, single-span beam, European train set

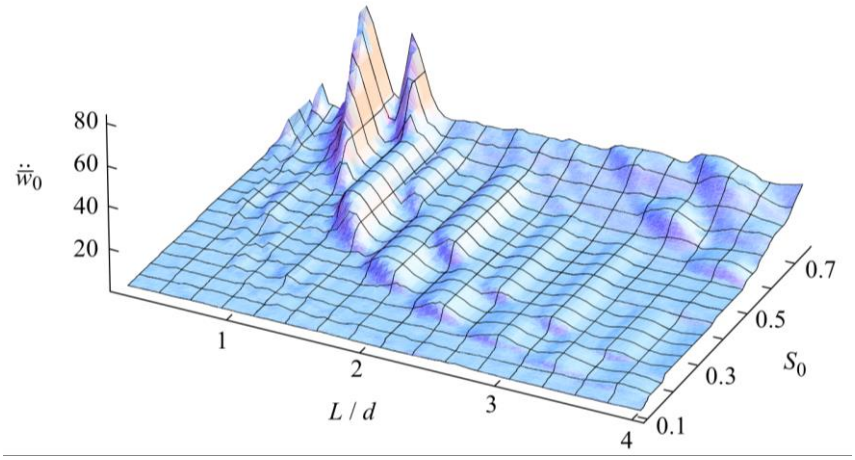

(b) Acceleration response spectrum, Two-span beam, European train set

Fig. 9 Acceleration response spectrum for the European train set. Prestressed concrete. (a) Single-span beam. (b) Two-span beam

response without performing time-expensive time history analyses considering various real bridges - train combinations.

5.3 Representation of response spectra

Exemplarily, in Fig. 9 three-dimensional envelope response acceleration spectrum for the European rail set are shown both for a single-span (Fig. 9(a)) and a two-span bridge (Fig. 9(b)) of prestressed concrete. Thus, according to Table 1 viscous damping is selected for prestressed concrete. The three-dimensional representation of the non-dimensional acceleration provides an excellent overview of the global response behavior. From Fig. 9(a) can be readily observed that there are domains of wave like local maxima, which are repeated periodically. For short bridges, i.e., for small length ratios *L*/*d*, there is a "wave crest", where the acceleration increases with a

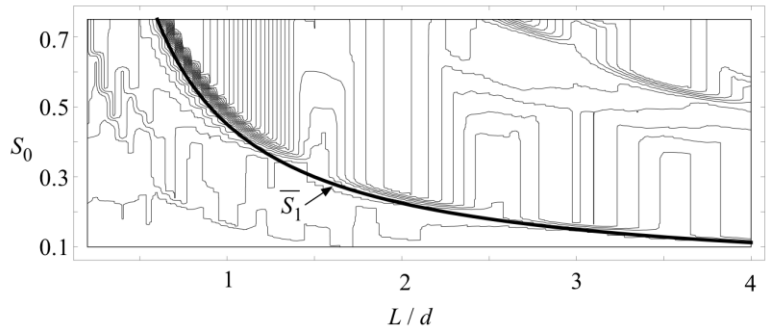

(a) Acceleration response, single-span beam, European train set

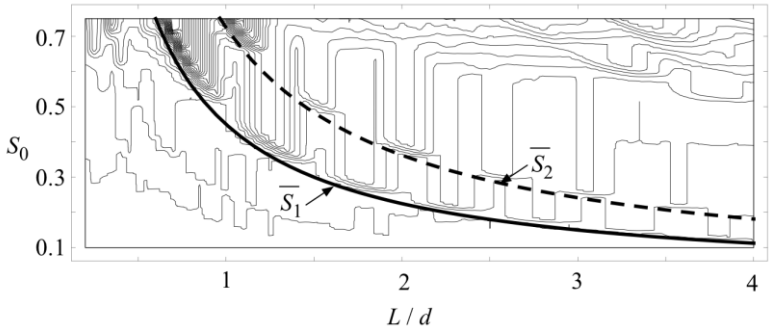

(a) Acceleration response, two-span beam, European train set

Fig. 10 Contour plot of the acceleration response spectrum for the European train set. Prestressed concrete. Functions $\overline{S}_1$ and $\overline{S}_2$, which separate the critical resonance domain from the less vulnerable domain with respect to resonance. (a) Single-span beam. (b) Two-span beam

sharp gradient until the maximum peak acceleration is attained. Furthermore, with increasing L/d the peak values are shifted to smaller values of S_0. Consequently, with increasing L/d trains with lower speeds may drive longer bridges into resonance.

Comparison of Figs. 9(a) and 9(b) reveals that there is a distinct difference in the response characteristics between a single-span and a two-span bridge. The total maximum peak acceleration in the displayed range of L/d and S_0 is larger for the single-span bridge. This outcome is reasonable, because the continuous transition of the two-span beam at the central support makes this structure stiffer compared to the single-span bridge. Moreover, in the two-span beam at low ratios L/d two "wave crest" with a sharp increase of the acceleration response can be seen separated by a "wavetrough", which does not exist for the single-span structure. Fig. 10 shows the corresponding contour plots of these response spectra.

Both in Fig. 10(a) and Fig. 10(b) a full line, which follows the empirically determined speed function

$$\overline{S}_1 = \frac{9}{10}\left(\frac{L}{d}\right)^{-1} \tag{15}$$

separates the critical resonance domain from the less vulnerable domain with respect to resonance. For speed parameters $S_0 > \overline{S}_1$ the response increases sharply due to resonance. In order to avoid

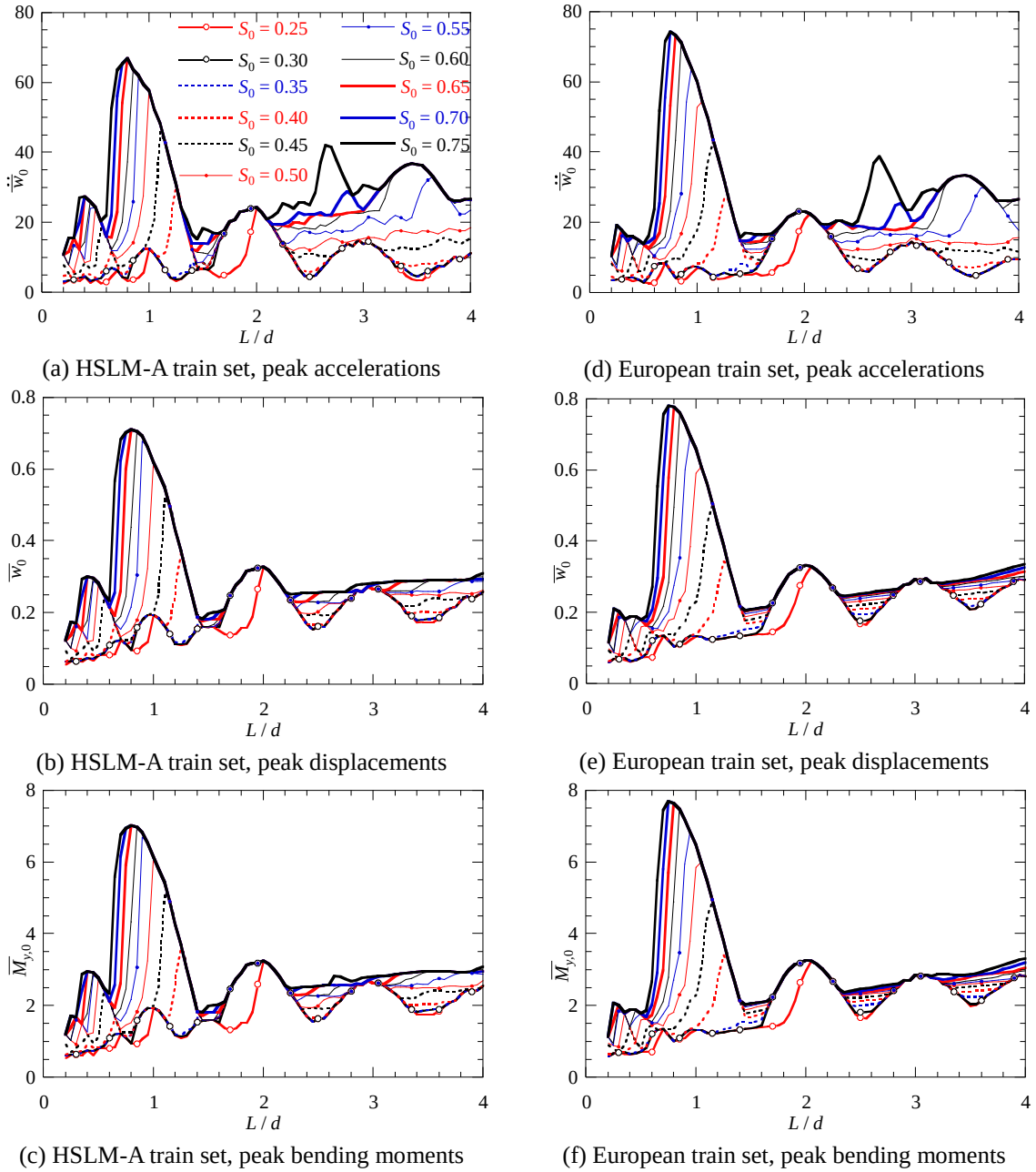

(a) HSLM-A train set, peak accelerations

(d) European train set, peak accelerations

(b) HSLM-A train set, peak displacements

(e) European train set, peak displacements

(c) HSLM-A train set, peak bending moments

(f) European train set, peak bending moments

Fig. 11 Response spectra displayed as function the length ratio L/d for selected values of the maximum admissible speed parameter S_0. Single-span beam. Prestressed concrete. Left column: Envelope spectra for the HLSM-A train set. Right column: Envelope spectra for the European train set. (a), (d) Normalized peak accelerations. (b), (e) Normalized peak displacements. (c), (f) Normalized peak bending moments

excessive dynamic response amplitudes it is recommended to design a railway bridge such that the maximum admissible speed parameter is smaller than the speed function $S_0 < \overline{S}_1$, if feasible.

Then, detailed dynamic analysis need not to be performed.

Additionally, for continuous two-span bridges with equal spans a second speed function can be identified empirically

$$\bar{S}_2 = \frac{29}{20}\left(\frac{L}{d}\right)^{-1} \tag{16}$$

Along this line, which is depicted in Fig. 10(b) by dashed line, a further sharp increase of the peak response can be observed. As it can be seen from Fig. 9(b) for values of $S_0 > \bar{S}_2$ additional "wave crests" arise.

Response spectra assist the practicing engineers in evaluating the expected dynamic peak response in the design process of railway bridges without performing time-consuming time history analyses. However, a two-dimensional representation of response spectra is more appropriate for practical applications. Thus, in Fig. 11 for single-span bridges made of prestressed concrete the non-dimensional peak response quantities displacement, acceleration, and bending moment are are plotted against the length ratio L/d for a series of discrete maximum admissible speed parameters S_0. In the left column the envelope spectra for the set of HLSM-A train models are displayed, the results of the right column are based on the set of European high-speed trains. The speed parameter considered starts at S_0=0.25 and ends at S_0=0.75, the length ratio L/d ranges between 0.2 and 4.0. These parameters cover "all" realistic bridges combined with "all" realistic train speeds. Note that the individual graphs of Figure 11(d) represent vertical sections of Figure 9(a) at constant values of S_0.

It is observed that the maximum response amplitudes are in the vicinity of L/d = 1. Further local maxima correspond to length ratios L/d of 2, 3 and 4. Peak acceleration spectra exhibit more local maxima than spectra of the displacements and bending moments. From this outcome it can be concluded that higher mode effects are more important for bridge accelerations. Comparison of the results in the left and the right column reveal that the maximum peak responses for the set of European trains are larger than for the HSLM-A train set. The difference is about 10% for all considered response quantities. However, some local maxima are larger for the set of HSLM-A trains. Thus, in the design process response spectra for both train sets should be utilized.

Alternatively, in Fig. 12 corresponding response spectra for the peak acceleration are illustrated as function of the maximum admissible speed parameter S_0 for selected values of the length ratio L/d. It can be seen that with increasing ratio L/d the peak values increase step-wise. However, this representation is less favorable compared to the one of Fig. 11, because in the presentation of Fig. 12 the global response behavior is "hidden".

In Fig. 13 two-dimensional envelope response spectra for two-span bridges for discrete values of S_0 are shown. Vertical sections of Fig. 9(b) at constant values of S_0 correspond to the results displayed in Fig. 13(b). Comparison of the results of the left and right column proves evidence that the European train set induce for all considered quantities the largest maximum peak response at L/d = 0.7. However, in particular for length ratios L/d larger than 1.5 there are domains, where the peak response due to the HSLM-A set is larger.

From the comparison of the individual non-dimensional response quantities derived for single-span and two-span bridges for a speed parameter of S_0 = 0.75 it can be observed that the peak response of a single-span beam is larger in almost the entire domain of considered ratios L/d, compare with Fig. 14. Thus, for a rough conservative check of the peak response spectra for single-span bridges can be utilized, if no spectra of two-span structures are available.

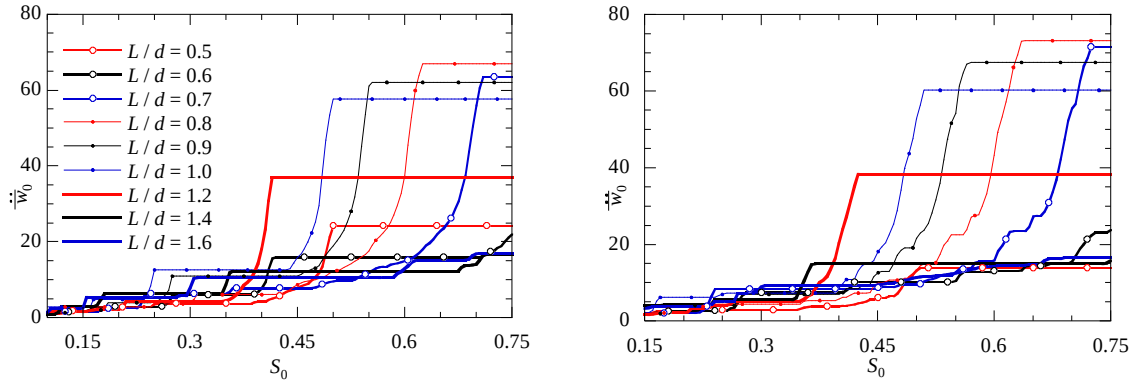

(a) HSLM-A train set (b) European train set

Fig. 12 Response spectra displayed as function of the maximum admissible speed parameter S_0 for selected values the length ratio L/d. Single-span beam. Prestressed concrete. Normalized peak accelerations. (a) Envelope spectra for the HSLM-A train set. (b) Envelope spectra for the European train set

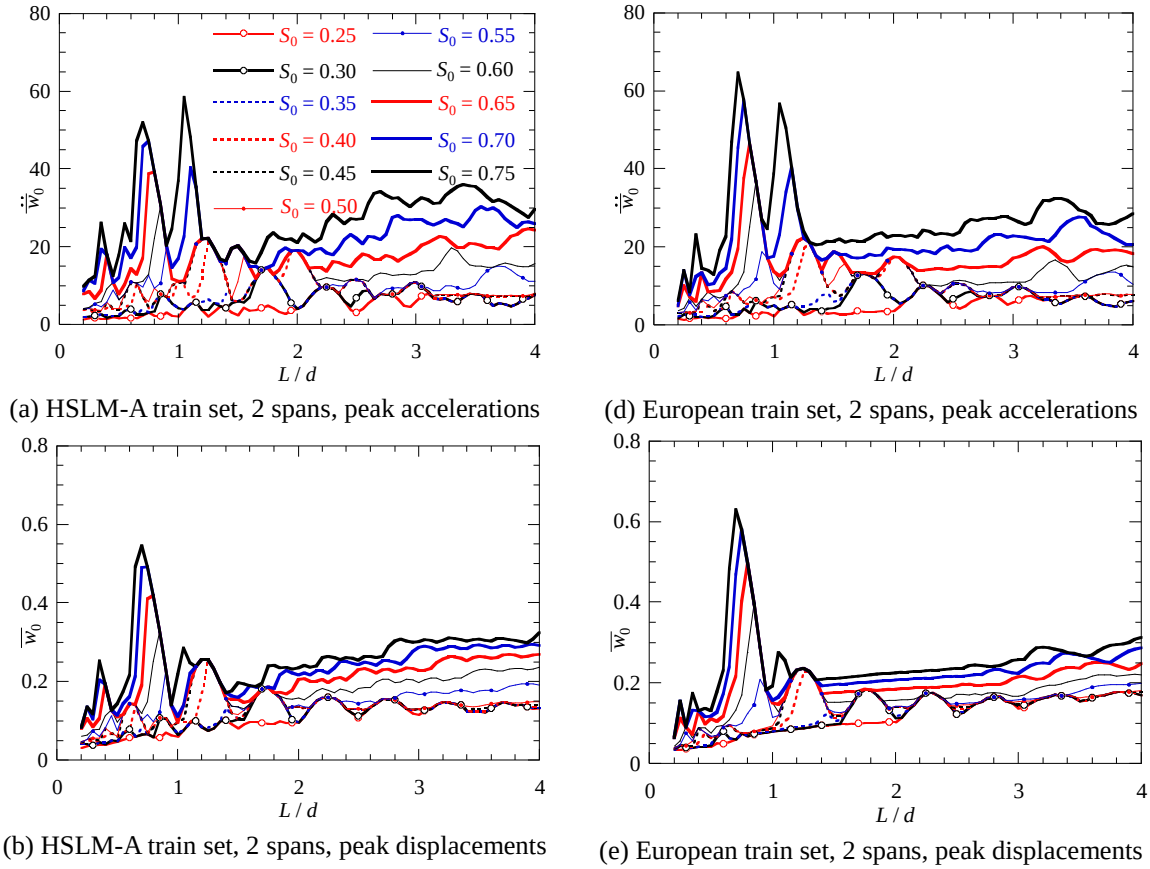

(a) HSLM-A train set, 2 spans, peak accelerations (d) European train set, 2 spans, peak accelerations

(b) HSLM-A train set, 2 spans, peak displacements (e) European train set, 2 spans, peak displacements

Fig. 13 Response spectra displayed as function the length ratio L/d for selected values of the maximum admissible speed parameter S_0. Two-span beam. Prestressed concrete. Left column: Envelope spectra for the HLSM-A train set. Right column: Envelope spectra for the European train set. (a), (d) Normalized peak accelerations. (b), (e) Normalized peak displacements. (c), (f) Normalized peak bending moments

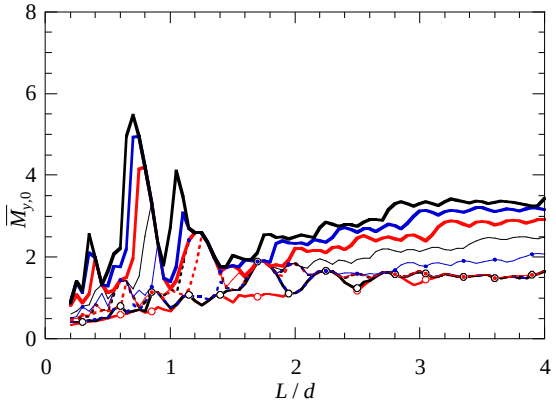

(c) HSLM-A train set, 2 spans, peak bending moment

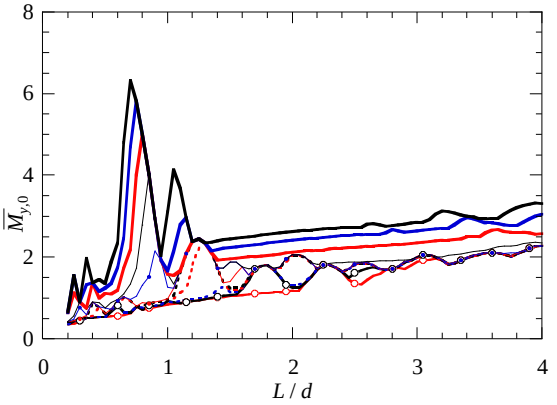

(f) European train set, 2 spans, peak bending moment

Fig. 13 Continued

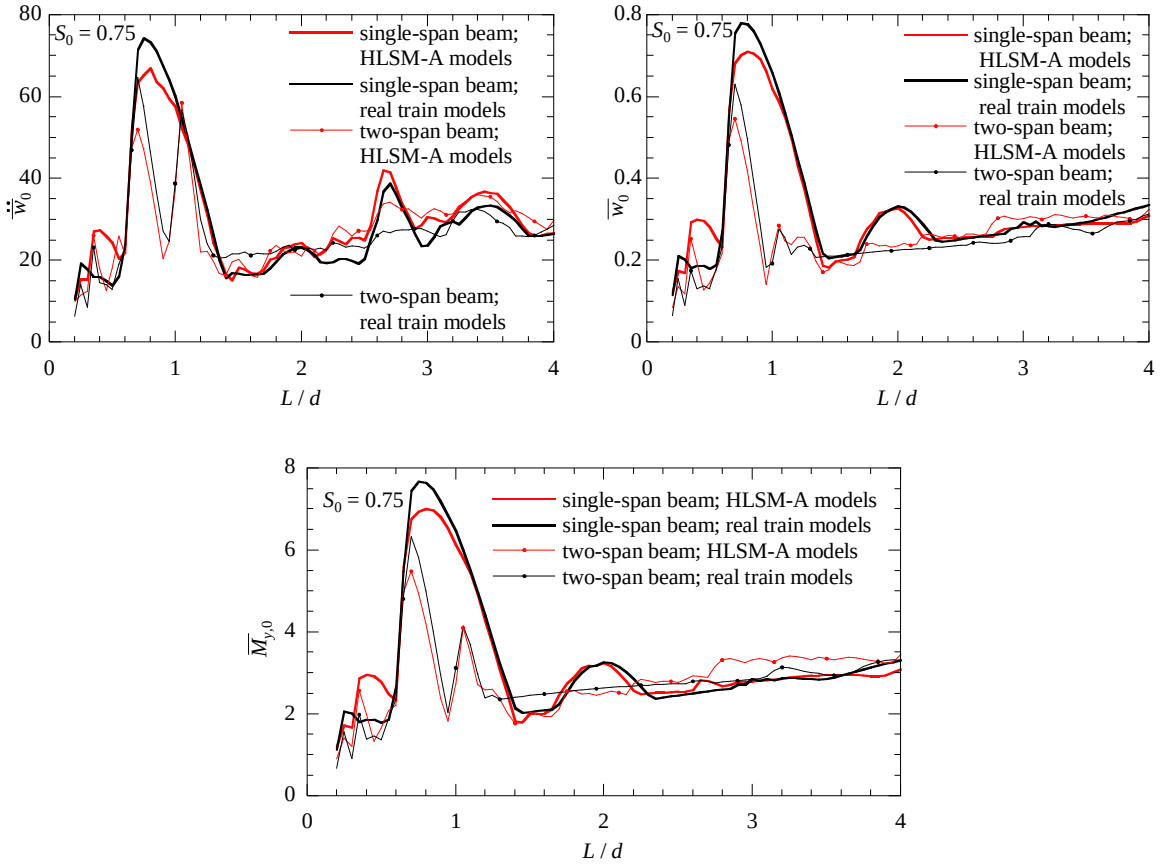

Fig. 14 Response spectra displayed as function the length ratio L/d for the maximum admissible speed parameter S_0=0.75. Single-span versus two-span beam. Prestressed concrete. Envelope spectra for the HLSM-A train set and for the European train set. (a) Normalized peak accelerations. (b) Normalized peak displacements. (c) Normalized peak bending moments

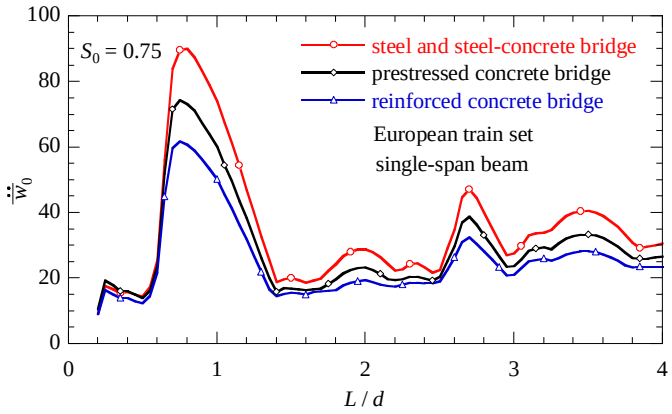

Fig. 15 Normalized peak accelerations as function the length ratio L/d for the maximum admissible speed parameter S_0=0.75. Single-span beam. Prestressed concrete. Variation of viscous damping according to Tabel 1

Table 1 Damping parameters according to Eurocode 1 (2003)

Bridge type	Viscous damping ζ_n [%], n =1, 2, 3,..	
	Span L<20 m	Span L≥20 m
Steel and steel-concrete composite	0.5 + 1.25 (20 – L)	0.5
Prestressed concrete	1.0 + 0.07 (20 – L)	1.0
Reinforced concrete	1.5 + 0.07 (20 – L)	1.5

Finally, the effect of viscous damping is quantified. Up to here, all presented results are based on the assumption that the bridges are made of prestressed concrete. According to Table 1, steel and steel-concrete bridges exhibit smaller viscous damping values, while damping of reinforced concrete is larger. Fig. 15 shows acceleration response spectra of a single-span bridge for a speed parameter S_0=0.75. The outcomes of steel and steel-concrete bridges, prestressed bridges, and reinforced concrete bridges are based on viscous damping ratios according to Table 1. Obviously, steel and steel-concrete bridges exhibit the largest peak responses. At length ratio $L/d = 0.8$ $\ddot{\bar{w}}_0 = 83.2$ for a steel and steel-concrete bridge, $\ddot{\bar{w}}_0 = 67.4$ for a prestressed concrete bridge, and $\ddot{\bar{w}}_0 = 56.3$ for reinforced concrete bridge. It is noted that response spectra for all damping coefficients specified in Table 1 can be found in (Salcher 2010).

5.4 Application

As an example problem the peak acceleration of a single-span prestressed concrete bridge with the following parameters is to be determined: L = 25.0 m, ρA = 20,000 kg/m, f_1 = 3.00 Hz. The train model HSLM-A4 passes the bridge (Eurocode 1 2003): d = 21 m, v_{max} = 250 km/h (= 69.4 m/s), F_{max} = 190,000 N. The design speed v_0 of the bridge corresponds to v_{max}. The non-dimensional input parameters can be derived as: L/d = 1.19, S_0 = 69.4/2/3.0/25 = 0.46 (compare with Eq. (12)). From response spectrum of Fig. 11(a) follows: $\ddot{\bar{w}}_0 \approx 40$. By rearranging the first of Eq. (13) from this value the expected peak bridge acceleration can be derived as

$$\max|\ddot{w}| = \ddot{\bar{w}}_0 \frac{F_{\max}}{\rho AL} = 40 \frac{190,000}{20,000 \times 25.0} = 15.2\,\mathrm{m/s}^2 \tag{17}$$

Accordingly, the peak displacement and peak bending moment can be determined utilizing the response spectra displayed in Figs. 11(b) and 11(c), respectively.

6. Conclusions

The presented study shows that higher modes may have a significant contribution on the dynamic acceleration response of bridges, in particular for the peak bridge acceleration of continuous two-span bridges. Merging the individual axle loads into a single concentrated force leads at resonance speeds to an over-conservative estimate of the bridge response. A novel representation of the non-dimensional dynamic peak response of railway bridges as function of a maximum admissible train speed parameter and a non-dimensional bridge length is introduced. The presented peak response spectra allow the practicing engineer a fast and yet accurate quantification of the dynamic peak response without conducting time-consuming and computationally expensive dynamic time history analyses.

References

Adam, C. (1999), "Forced vibrations of elastic bending-torsion coupled beams", *J. Sound Vib.*, **221**(2), 273-287.

Adam, C., Heuer, R., Raue, A. and Ziegler, F. (2000), "Thermally induced vibrations of composite beams with interlayer slip", *J. Thermal Stresses*, **23**, 747-772.

Blevins, R.D. (1979), *Formulas for Natural Frequency and Mode Shape*, Krieger Publishing Company.

Clough, R.W. and Penzien, J. (1993), *Dynamics of Structures*, 2nd Edition, McGraw-Hill.

Eurocode 1 (2003), *Actions on structures. Part 2: General actions - Traffic loads on bridges*, EN 1991-2, Brussels.

Fink, J. and Mähr, T. (2007), "Simplified method to calculate the dynamic response of railway-bridges on the basis of response spectra", *Proceedings 6th International Conference on Bridges across the Danube* (Eds. Ivanyi, M. and Bancila, R.), Budapest, Hungary, September.

Fryba, L. (1996), *Dynamics of Railway Bridges*, Thomas Telford, London, UK.

Fryba, L. (2001), "A rough assessment of railway bridges for high speed trains", *Eng. Struct.*, **23**, 548-556.

Hauser, A. and Adam, C. (2007), "Abschätzung der Schwingungsantwort von Brückentragwerken für Hochgeschwindigkeitszüge", *Proceedings D-A-CH Tagung 2007 der Österreichischen Gesellschaft für Erdbebeningenieurwesen und Baudynamik*, Vienna, Austria, September. (in German)

Museros, P. and Alarcon, E. (2005), "Influence of the second bending mode on the response of high-speed bridges at resonance", *J. Struct. Eng.*, ASCE, **131**, 405-415.

Liu, K., De Roeck, G. and Lombaert, G. (2009), "The dynamic effect of the train-bridge interaction on the bridge response", *Proceedings COMPDYN 2009 - Conference on Computational Methods in Structural Dynamics and Earthquake Engineering*, (Eds. Papadrakakis, M., Lagaros, N.D. and Fragiadakis, M.), Rhodes, Greece, June.

Salcher, P. (2010), *Dynamic effect of high-speed trains on simple bridges*, Diploma Thesis, University of Innsbruck. (in German)

Wang, Y., Wei, Q.C., Shi, J. and Long, X. (2010), "Resonance characteristics of two-span continuous beam under moving high speed train", *Lat. Am. J. Solid. Struct.*, **7**, 185-199.

Xia, H., Zhang, N. and Guo, W.W. (2006), "Analysis of resonance mechanism and conditions of train -

bridge system", *J. Sound Vib.*, **297**, 810-822.
Yang, Y.B., Yau, J.D. and Hsu, L.C. (1997), "Vibration of simple beams due to trains moving at high speeds", *Eng. Struct.*, **19**, 936-944.
Yang, Y.B., Yau, J.D. and Wu, Y.S (2004), *Vehicle-Bridge Interaction Dynamics: With Applications to High-Speed Railways*, World Scientific Publishing, Singapore.
Zambrano, A. (2011) "Determination of critical loading conditions for bridges under crossing trains", *Eng. Struct.*, **33**, 320-329.
Ziegler, F. (1998), *Mechanics of Solids and Fluids*, corrected reprint of the 2nd Edition, Springer, New York, Vienna.